J Neurophysiol 92: 2283–2294, 2004;
10.1152/jn.00109.2004.

Threshold Firing Frequency–Current Relationships of Neurons in Rat Somatosensory Cortex: Type 1 and Type 2 Dynamics

T. Tateno, A. Harsch, and H.P.C. Robinson
Department of Physiology, University of Cambridge, Cambridge CB2 3EG, United Kingdom

Submitted 3 February 2004; accepted in final form 20 May 2004

Tateno, T., A. Harsch, and H.P.C. Robinson. Threshold firing frequency–current relationships of neurons in rat somatosensory cortex: type 1 and type 2 dynamics. *J Neurophysiol* 92: 2283–2294, 2004; 10.1152/jn.00109.2004. Neurons and dynamical models of spike generation display two different types of threshold behavior, with steady current stimulation: type 1 [the firing frequency vs. current (*f–I*) relationship is continuous at threshold) and type 2 (discontinuous *f–I*)]. The dynamics at threshold can have profound effects on the encoding of input as spikes, the sensitivity of spike generation to input noise, and the coherence of population firing. We have examined the *f–I* and frequency–conductance (*f–g*) relationships of cells in layer 2/3 of slices of young (15–21 DIV) rat somatosensory cortex, focusing in detail on the nature of the threshold. Using white-noise stimulation, we also measured firing frequency and interspike interval variability as a function of noise amplitude. Regular-spiking (RS) pyramidal neurons show a type 1 threshold, consistent with their well-known ability to fire regularly at very low frequencies. In fast-spiking (FS) inhibitory interneurons, although regular firing is supported over a wide range of frequencies, there is a clear discontinuity in their *f–I* relationship at threshold (type 2), which has not previously been highlighted. FS neurons are unable to support maintained periodic firing below a critical frequency f_c, in the range of 10 to 30 Hz. Very close to threshold, FS cells switch irregularly between bursts of periodic firing and subthreshold oscillations. These characteristics mean that the dynamics of RS neurons are well suited to encoding inputs into low-frequency firing rates, whereas the dynamics of FS neurons are suited to maintaining and quickly synchronizing to gamma and higher-frequency input.

INTRODUCTION

In a study of the responses of axons isolated from *Carcinus meanas* to various intensities of rectangular current stimuli, Hodgkin found that some axons could be induced to fire at a frequency that varied smoothly over a large range as stimulus intensity varied, whereas others were relatively insensitive to stimulus intensity (Hodgkin 1948). The discharge frequencies of this latter type lay within a narrow range, clearly distinct from zero. From these observations, and previous work on other preparations, such as *Cancer pagurus* axons (Arvanitaki 1936) and decalcified nerves of frogs and squids (Brink et al. 1946), Hodgkin separated excitable membranes into two "classes," which have more recently been referred to as "types." The crucial distinction is that, whereas type 1 neurons show a *continuous* transition from zero frequency to arbitrarily low frequencies of firing, type 2 neurons show an *abrupt* onset of repetitive firing at a *nonzero* firing frequency. Clearly, all continuously firing neurons with a threshold will fall into one of these 2 types, which thus represent the behavior of a wide range of excitable membranes.

Even simple dynamical models of spike generation can exhibit both kinds of behavior, depending on their parameters (Morris and Lecar 1981; Rinzel and Ermentrout 1998). In these models, because of the different natures of dynamical bifurcation at threshold, type 1 behavior is associated with all-or-nothing spikes, whereas type 2 behavior is associated with graded spike amplitude and subthreshold oscillations. Recently, modeling studies have shown that the threshold type of the neuron profoundly affects the reliability of spike generation in the presence of noise (Gutkin and Ermentrout 1998; Robinson and Harsch 2002). Experimental classification of the responses of neurons in the cortex, however, has focused mostly on the form of the frequency vs. current (*f–I*) relationship in responses that are well above threshold (Connors and Gutnick 1990; Kawaguchi and Kubota 1997; Nowak et al. 2003); a clear classification of the continuity or discontinuity of the *f–I* relationship at threshold is lacking. Therefore in this paper we study the thresholds of 2 well-characterized types of cell—regular-spiking and fast-spiking neurons—and show that they follow type 1 and type 2 behaviors, respectively. We discuss what impact this could have on the roles of these 2 cell types in the cortical network.

METHODS

Slice preparation and recording

Transverse slices were prepared from somatosensory cortex of 15- to 21-day-old Wister rats using standard techniques (Sakmann and Stuart 1995). During slicing, tissue was kept in sodium-free solution that had the following composition (in mM): 254 sucrose, 2.5 KCl, 26 $NaHCO_2$, 10 glucose, 1.25 NaH_2PO_4, 2 $CaCl_2$, and 1 $MgCl_2$. Slices of 300 μm thickness were cut on a vibrating slicer (Microslicer DTK-3000, D.S.K., Kyoto, Japan) and kept in Ringer solution at room temperature for $\geq$2 h before recording. The Ringer solution contained (in mM):125 NaCl, 2.5 KCl, 25 $NaHCO_2$, 25 glucose, 1.25 NaH_2PO_4, 2 $CaCl_2$, and 1 $MgCl_2$. Both slicing and recording solutions were equilibrated with 95% O_2,-5% CO_2 gas to a final pH of 7.4. Slices were viewed with an upright microscope (Olympus BW50WI, Olympus UK, London) using infrared differential interference contrast optics. All experiments were performed at 30 $\pm$ 1°C. Whole cell patch-clamp recordings were made from the somas of neurons in layers 2/3. Putative regular-spiking cells were of pyramidal morphology, whereas putative fast-spiking cells were selected on the basis of a nonpyramidal shape and multipolar dendrites (Connors et al. 1982). During recording, the slices were perfused continuously with Ringer solution in which 10 μM bicuculline, 10 μM CNQX, and 10 μM AP5

Present affilitation and address for reprint request: T. Tateno, Department of Mechanical Science and Bioengineering, Graduate School of Engineering Science, Osaka University, 1-3 Machikaneyama, Toyonaka, Osaka 560-8531, Japan.

The costs of publication of this article were defrayed in part by the payment of page charges. The article must therefore be hereby marked "*advertisement*" in accordance with 18 U.S.C. Section 1734 solely to indicate this fact.

(Tocris Cookson, Bristol, UK) were included to block most intrinsic synaptic conductances. However, some activity and synaptic input appeared to persist because there were typically still small fluctuations (1–2 mV) in the membrane voltage at the current-clamp mode. Somatic patch-pipette recordings were made with a Multiclamp 700A amplifier (Axon Instruments, Foster City, CA) in current-clamp mode, correcting for prenulled liquid junction potential. Whole cell recording pipettes (Clark GC150T-7.5) with 3.9–4.3 MΩ were filled with the standard intracellular solution: 105 mM K gluconate, 30 mM KCl, 10 mM HEPES, 10 mM phosphocreatine Na_2, and 0.3 mM Na-GTP, balanced to pH 7.3 with NaOH. Series resistance compensation was used.

For conductance injection (dynamic-clamp) stimulation (Robinson and Kawai 1993; Sharp et al. 1993), an SM-1 conductance injection amplifier (Cambridge Conductance, Cambridge, UK) was used to inject step commands of ohmic excitatory conductance (reversal potential −10 mV) or mixtures of excitatory and inhibitory shunting conductance (reversing at the resting potential). Signals were filtered at 5 kHz and sampled with 12-bit resolution at 20 kHz. For stochastic stimulation, the sum of a constant current (I_0) and a white Gaussian noise current [$\xi(t)$] was used; i.e., the stimulus current $I(t)$ is described by $I(t) = I_0 + \sigma\xi(t)$, where σ is the noise intensity. I_0 was set to be just below the spike threshold of each cell so that no spike occurred in the absence of the noise term. This parameter regime is referred to as "excitable," whereas the parameter regime in which repetitive firing occurs is referred to as "oscillatory." In each run, a 10-s stimulus $I(t)$ was repeatedly applied to cells 20 to 30 times, separated by 40-s recovery intervals, but each noise realization was different. In a test for temperature sensitivity, we measured from 6 cells (3 RS, 3 FS) at temperatures of 30, 34, and 37°C, and found no significant difference in critical frequency (f_c) and maximal firing frequency (f_{max}) in any cell. Thus variations in temperature over this range did not seem to be a major factor shaping the threshold dynamics.

Spike statistics

Action potential shape parameters were measured from action potentials evoked by just-suprathreshold 200-ms current steps from a resting membrane potential near −70 mV. Spike amplitude was measured as the difference between the peak and the threshold of the action potential. *Spike threshold* was defined as the potential at which the first derivative of the voltage waveform exceeded 8 times its baseline SD. The afterhyperpolarization (AHP) was measured as the difference between the spike threshold and voltage minimum following the action potential peak. Spike width was measured at half the spike amplitude. Spike times were measured as the times of upward zero crossing of the membrane potential. Instantaneous frequency (reciprocal of interspike interval) was computed from trains of action potentials evoked by 600-ms duration pulses for the 1st, 2nd, and 4th interspike intervals. Steady-state (SS) firing frequency was computed as the average of instantaneous frequency for the last 5 intervals of a train. Current or conductance strength was usually progressively increased or decreased in small (10-pA or 500-pS) steps. Initial instantaneous frequency and SS firing rate were plotted as a function of the injected current or conductance strength, to construct frequency–current (*f–I*) or frequency–conductance (*f–g*) relationships. *f–I* relationships were fitted to the simple function $f = (aI - b)^d$ ($I > b/a$, $0 < d \leq 1$), where f and I respectively represent firing frequency and current intensity and a, b, and d are constant parameters. A similar function was used by Ermentrout (1998). When d is close to 1, the *f–I* relationship is linear; if d is close to 0, it becomes markedly nonlinear (sublinear). The maximum firing rate of a neuron was computed from the number of spikes per trial at the highest current strength before depolarization block. The frequency adaptation properties of neurons were characterized by calculating the instantaneous firing rate as a function of time since the beginning of the 600-ms pulse. For each current intensity, the decay of firing rate was fitted to a single exponential function

$$f = C\exp(-t/\tau_a) + F_a \quad (1)$$

where f and t represent the firing rate and time after the stimulus onset, respectively, and C, τ_a, and F_a are positive constant parameters. F_a represents the adapted firing rate. The strength of adaptation (adaptation index, A) was quantified as $100 \times (1 - F_a/F_1)$, where F_1 corresponds to the firing rate of the 1st interspike interval. For a given neuron, because the parameters of the firing rate curve strongly depend on the current intensity, the highest current level not producing depolarization block of spiking was used for comparison among cells. For some cells, no adequate exponential fit could be obtained. For these cells, F_a was calculated as the mean firing rate for the last 50 ms of the 600-ms current pulse and used to calculate the adaptation index. Results are reported as means ± SD.

Estimating membrane impedance and frequency characteristics

Membrane impedance characteristics were estimated in both the time domain and the frequency domain. In the time domain, membrane time constants were obtained by fitting a single exponential function to the initial part of more than 10 time-averaged voltage responses to small (−20 or −10 pA), 600-ms-long hyperpolarizing current pulses. Input resistance was calculated from Ohm's law by dividing the maximal average voltage deflection by the amplitude of the applied current pulses. In the frequency method, a 20-s-long sinusoidal current with a frequency varying linearly from 0 to 32 or 128 Hz (ZAP function) was used as the stimulus (Gutfreund et al. 1995), and a maximal amplitude was set just below the threshold for producing spikes. To estimate the magnitude of the impedance, the current (I) and voltage (V) recordings were converted to the frequency domain by fast Fourier transform. Impedance (Z) was calculated from the coefficients of Fourier transforms. In complex polar notation, the impedance is expressed in terms of its magnitude $|Z(f)|$ and phase $\theta(f)$

$$Z = |Z(f)|e^{-j\theta(f)} \quad (2)$$

where f is frequency. The magnitude [$|Z(f)|$] and phase [$\theta(f)$] of the complex-valued impedance were plotted against frequency to give impedance-magnitude (IM) and impedance-phase (IP) profiles respectively. Subthreshold IM and IP profiles of individual neurons were compared with those expected for a passive membrane circuit with the same input resistance and time constant

$$|Z(f)| = R_i/\sqrt{(\tau_i^2(2\pi f)^2 + 1)} \quad (3)$$

where R_i is input resistance and τ is the membrane time constant, and

$$\theta(f) = -\arctan(2\pi f\tau_i) \quad (4)$$

Input resistance and membrane time constant were calculated by fitting the impedance magnitude–frequency relationship using a standard method of least squares (function lsqcurvefit in Optimization Toolbox, MATLAB, The MathWorks, Natick, MA).

Numerical calculation of neural models

f–I curves of neural models were constructed with AUTO (Doedel and Kernevez 1986), a component of XPPAUT software (Ermentrout 2002). To simulate neural models in an excitable regime driven by white Gaussian noise, we used the forward improved Euler or Heun method (Kloeden 1999), with a time step of $\Delta t = 1$ μs. This method gives a higher-order discretization error than that of the simple Euler method. The stimulus current $I(t) = I_0 + \sigma\xi(t)$ was set in the excitable regime, as described above for the experiments. To calculate coeffi-

cient of variation (SD/mean) of interspike intervals, a fixed-voltage threshold was used to detect spikes, but the exact level used had no significant effects on the results.

RESULTS

Separation of cell types in rat somatosensory cortex

Based on responses to current-step injection, cells recorded in layer 2 or 3 of somatosensory cortex were classified into 2 groups: regular-spiking (RS) and fast-spiking (FS) cells. RS cells had a typical pyramidal morphology under infrared differential interference contrast optics (Fig. 1*A*), whereas FS cells were selected on the basis of a nonpyramidal shape and a round soma with multipolar dendrites (Fig. 2*A*). This study is based on recordings from 20 RS neurons and 23 FS neurons.

Figure 1*B* shows typical spiking responses of an RS neuron when a 600-ms current step was injected, at 3 different amplitude levels. RS neurons had an average resting potential of -71.8 ± 3.5 mV. They had an average input resistance of 424.0 ± 189.7 MΩ and a time constant of 41.2 ± 12.5 ms estimated in the time domain (see METHODS). When estimated in the frequency domain (see METHODS) (Fig. 1*C*), the average input resistance was 349.7 ± 165.2 MΩ and the average time constant was 40.2 ± 10.5 ms. RS neurons showed long-duration action potentials (1.71 ± 0.36 ms) and small AHPs (7.3 ± 2.4 mV), as shown in Fig. 1*B*. In response to sustained current injection, RS cells showed a relatively low maximum frequency firing (32.3 ± 7.0 Hz). In addition, RS cells showed substantial spike broadening between the 1st and 2nd action potentials of a train, with an average 2nd spike width of 2.22 ± 0.50 ms.

Figure 2*B* shows spike responses of FS neurons. These had an average resting potential of -71.2 ± 4.0 mV. They had an average input resistance of 357.4 ± 147.5 MΩ and a time constant of 29.7 ± 5.9 ms when estimated in the time domain, and input resistance of 229.3 ± 73.1 MΩ and time constant of 21.8 ± 9.2 ms estimated in the frequency domain. One of the reasons for the relatively larger discrepancies between time and frequency domain estimates of membrane parameters in FS cells is that the subthreshold impedance characteristics of FS cells could not always be well modeled by an RC circuit. They also had shorter-duration action potentials (1.18 ± 0.17 ms, $P < 0.001$) and larger AHPs (17.1 ± 4.1 mV, $P < 0.001$) than those of RS cells. FS cells had a much higher maximum frequency firing (61.0 ± 9.1 Hz, $P < 0.001$). They showed no substantial spike broadening between the 1st and 2nd action potentials of a train: the average 2nd spike width was 1.25 ± 0.18 ms, shorter than that of RS cells ($P < 0.001$).

A scatter-plot comparison of spike-shape parameters (AHP, the 2nd spike width, and *A*) versus maximal firing frequency for all cells revealed bimodal distributions of parameters, with little overlap between RS and FS cells, as shown in Fig. 3.

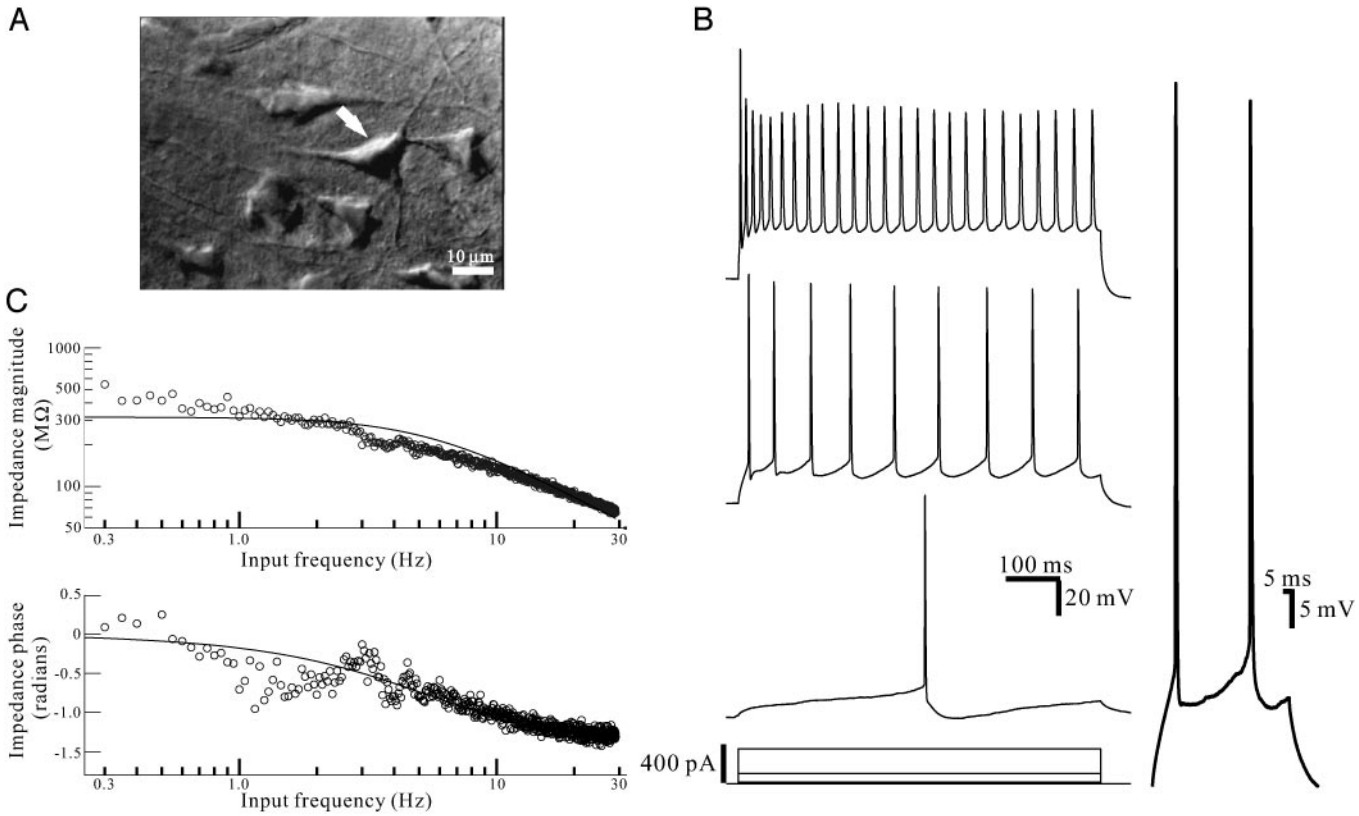

FIG. 1. Subthreshold and firing properties of regular spiking neurons in layer 2/3 somatosensory cortex. *A*: photomicrograph of a typical regular-spiking (RS) neuron, with pyramidal morphology. *B*: repetitive firing of RS cells for 3 different current steps of increasing amplitude (90–380 pA). Suprathreshold current injection produced repetitive firing at comparatively lower frequencies and with substantially more spike frequency adaptation than observed for fast-spiking (FS) cells (cf., Fig. 2*B*). *Right panel*: RS cells had broad 1st action potentials and showed further broadening between 1st and 2nd spikes (stimulus: 200-ms just-suprathreshold current of 80 pA). *C*: *top*: impedance magnitude as a function of frequency for an RS cell. *Bottom*: impedance phase as a function of frequency for the same cell.

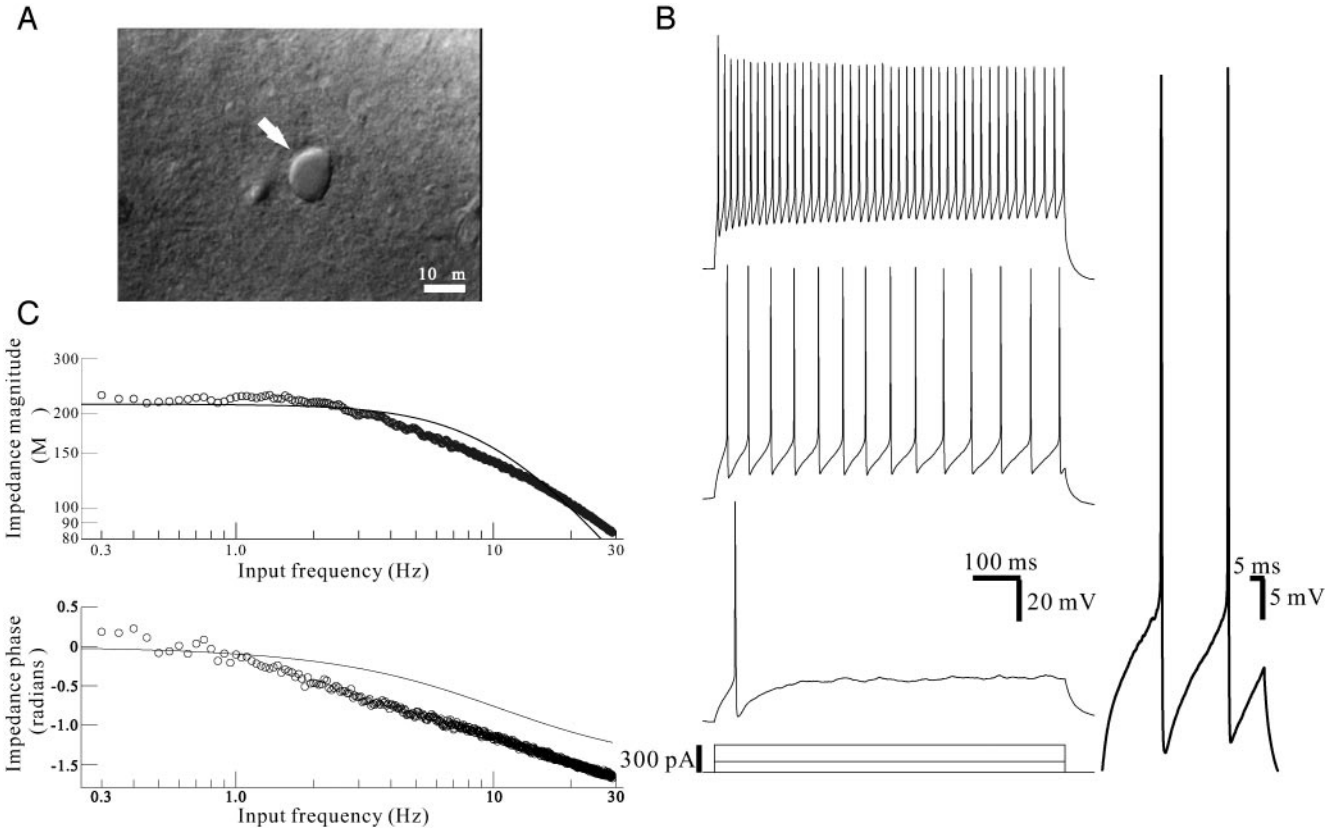

FIG. 2. Subthreshold and firing properties of FS neurons in layer 2/3 somatosensory cortex. *A*: photomicrograph of a typical FS neuron, with round morphology. *B*: repetitive firing of FS cells for 3 different current steps of increasing amplitude (70–300 pA). Repetitive firing had an abrupt onset in FS cells. In response to a just-suprathreshold 600-ms step current, the FS cell fired a single spike before adapting. Repetitive firing began at a critical frequency (about 20 spikes/s) in response to an 80-pA current step. *Right panel*: FS cells had shorter duration action potentials, with less variation between 1st and 2nd spikes, and larger afterhyperpolarizations (AHPs) than those in RS cells (stimulus: 65 pA for 200 ms). *C*: *top*: impedance magnitude as a function of frequency for an FS cell. *Bottom*: impedance phase as a function of frequency for the same cell.

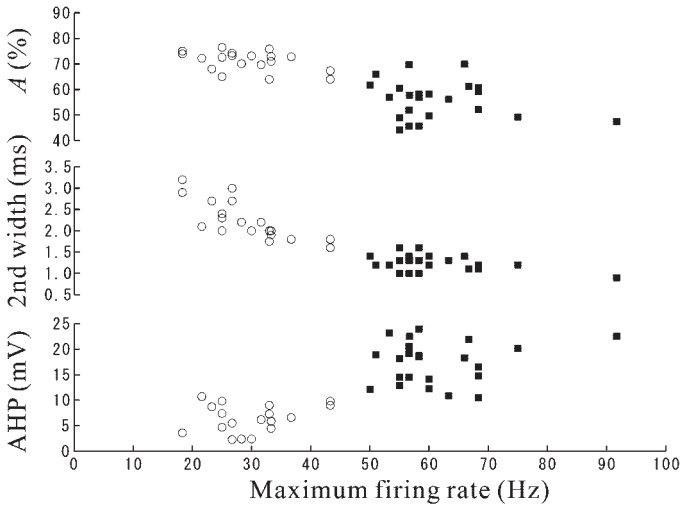

FIG. 3. Spike and firing parameters for RS (circles) and FS (filled squares) cells. AHP amplitude of the 1st spike, width of 2nd action potential (2nd width), and the adaptation index are plotted against the maximum firing frequency. Cells were classified into 2 clear types, RS and FS, which were almost completely segregated in AHP, A1, and 2nd width, and completely segregated in maximum firing rate. Similar plots can be found in Fig. 2*E* of Erisir et al. (1999).

Thus RS and FS neurons were reliably distinguished from each other on the basis of firing frequency, adaptation, and spike shape. The statistics for each cell type, together with significance levels for the differences between types, are shown in Table 1.

f–I relationships of RS and FS neurons

In response to sustained current injection, RS cells showed a strong frequency adaptation ($A = 71.4 \pm 4.2$) with a decay time constant (τ_a) of 29.5 ± 9.5 ms, as shown in Fig. 4*A*. Figure 4*B* shows that their *f–I* relationship is continuous at threshold. The lowest frequencies approached the lowest measurable limit given the duration of the stimulus (1.66 Hz). In general, values slightly higher than this limit are expected, given the finite current increments used. For the 1st instantaneous and SS firing frequency versus current relationships, the average powers of the dependency of f on I [i.e., the exponent d in a fit to the relationship $f = (aI - b)^d$; see METHODS] were respectively 0.84 ± 0.12 and 0.57 ± 0.12. The 1st interspike interval presumably reflects the instantaneous firing rate before substantial activation of an adaptation mechanism that has a nonlinear dependency on I. Thus the 1st instantaneous rate has a weaker nonlinearity than the SS firing *f–I* relationship.

TABLE 1. *Summary of statistics on RS and FS cells*

Parameter	Regular-Spiking	Fast-Spiking	*P*
Number of cells	20	23	
Maximum firing rate, Hz	32.3 ± 7.0	61.0 ± 9.1	<0.001
Resting potential, mV	−71.8 ± 3.5	−71.2 ± 4.0	—
Input resistance, MΩ	424.0 ± 189.7	357.4 ± 147.5	—
Time constant, ms	41.2 ± 12.5	29.7 ± 5.9	<0.005
Spike amplitude, mV	78.1 ± 9.0	72.8 ± 6.5	<0.05
AHP amplitude, mV	7.3 ± 2.4	17.1 ± 4.1	<0.001
1st spike width (W_1), ms	1.71 ± 0.36	1.18 ± 0.17	<0.001
2nd spike width (W_2), ms	2.22 ± 0.50	1.25 ± 0.18	<0.001
Adaptation index (A)	71.4 ± 4.2	56.2 ± 6.7	<0.001
Adaptation decay time constant (τ_a), ms	29.5 ± 9.5	54.2 ± 33.8	<0.05
R_i, MΩ	349.7 ± 165.2	229.3 ± 73.1	<0.05
τ_i, ms	40.2 ± 10.53	21.8 ± 9.2	<0.001
d_1	0.84 ± 0.12	0.65 ± 0.13	<0.001
d_{ss}	0.57 ± 0.12	0.36 ± 0.12	<0.001

Values are means ± SD. Significant differences between the RS and FS groups are indicated in *P*. RS, regular spiking; FS, fast spiking; AHP, afterhyperpolarization; SS, steady state; R_i, input resistance estimated by impedance amplitude; τ_i time constant estimated by impedance amplitude; d_1, the power parameter d of the approximation of the *f–I* curve by $f = (aI - b)^d$ for the 1st instantaneous firing frequency; d_{ss}, for SS firing frequency.

In contrast, FS cells showed relatively little frequency adaptation ($A = 56.2 \pm 6.7$, $P < 0.001$) with a longer decay time constant (τ_a) of 54.2 ± 33.8 ms ($P < 0.05$) (Fig. 4*C*). They were able to fire at high frequencies with relatively little spike frequency adaptation, which occurred mainly over the first few spikes. They also showed an abrupt onset of repetitive firing with increasing current, as shown in Fig. 4*D*. There is a clear discontinuity at a critical frequency f_c in their *f–I* relationship at threshold. FS neurons are unable to support maintained regular firing below the critical frequency, which varied between 10 and 30 Hz for different cells. Above f_c, the instantaneous firing rate increased monotonically with current strength. In some cases, however, the relation reached a clear plateau at current strengths below those that caused spike failure. For the 1st instantaneous and SS *f–I* relationships, average *d* values of fits were 0.65 ± 0.13 and 0.36 ± 0.12, both significantly smaller than for RS cells ($P < 0.001$). Note that the maximum firing frequency for FS cells (≤100 Hz) is lower than that reported in some other studies (Erisir et al. 1999; Kawaguchi 1995). We ascribe this to the comparatively young age of slices used here.

Firing frequency and conductance input

During the normal operation of cortical neurons in the intact animal, the stimulus consists of the conductance of synaptic receptor channels, a current source that reacts to the membrane potential, and which can greatly alter the input resistance and membrane time constant of cells (Destexhe et al. 2001) and cause considerable shunting of action potential amplitude. To test whether this affects the classification of RS and FS cells' threshold behaviors, we used the conductance injection or dynamic-clamp technique (Robinson and Kawai 1993; Sharp et al. 1993) to stimulate action potential firing by step commands of ohmic excitatory conductance (reversal potential −10 mV) or mixtures of excitatory and inhibitory shunting conductance (reversing at the resting potential). Figure 5 shows responses of RS neurons to conductance stimulation. Either AMPA-type conductance alone (Fig. 5*A*, *left*) or in the presence of shunting, GABA-type conductance (Fig. 5*A*, *right*), produced an increasing firing frequency as the excitatory stimulus was increased. Interestingly, the firing frequency–conductance (*f–g*) relationship of instantaneous firing frequency showed a pronounced shift to the right with increasing shunting (Fig. 5*B*), whereas the SS *f–g* relationship was much less sensitive (Fig. 5*C*) at higher levels of excitation, possibly reflecting the activation of an additional intrinsic conductance, attenuating the effect of the injected GABA-type conductance. As with current stimu-

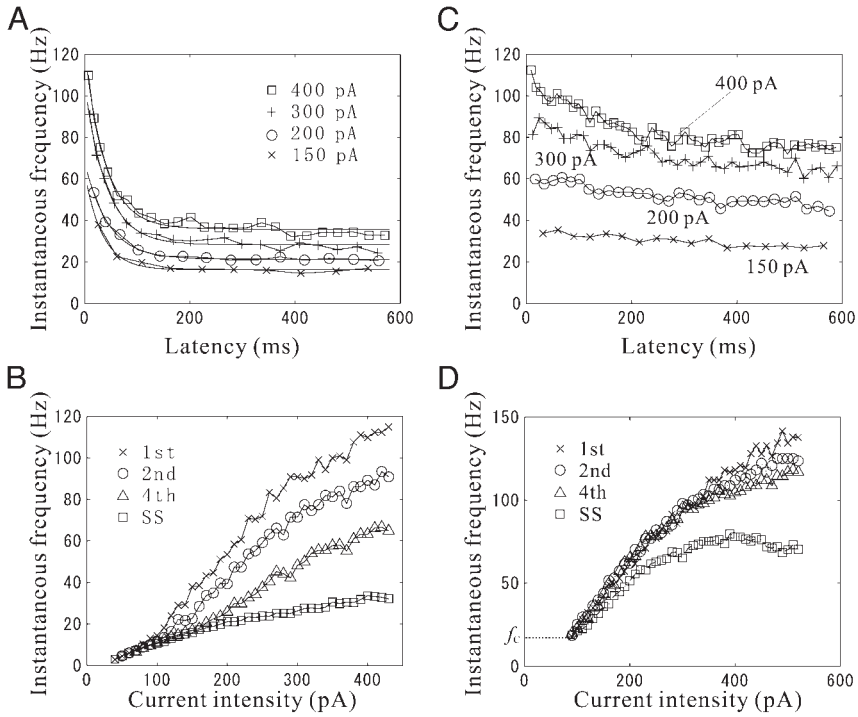

FIG. 4. Instantaneous firing frequency of RS and FS cells. *A*: RS neuron: instantaneous firing frequency (1/interspike interval) vs. time after onset of current pulse, showing strong frequency adaptation. At each of 4 selected current strengths (150, 200, 300, and 400 pA), the curves were well fitted by a single exponential decay (τ_a = 17.0, 21.7, 25.6, and 29.1 ms, respectively). *B*: RS neuron *f–I* relationship. Frequencies corresponding to the 1st, 2nd, and 4th intervals and the steady-state (SS) frequency increased monotonically with the current strength, starting from 2 to 4 spikes/s, as low as could be assessed with this stimulus duration. *C*: FS neuron, instantaneous firing frequency vs. time relationship, showing only slight frequency adaptation at 4 different stimulus currents, as indicated, increasing with current strength. *D*: FS neuron *f–I* relationship. Frequency increases with current strength above a critical frequency f_c (~20 spikes/s). SS frequency reaches a plateau at about 350 pA.

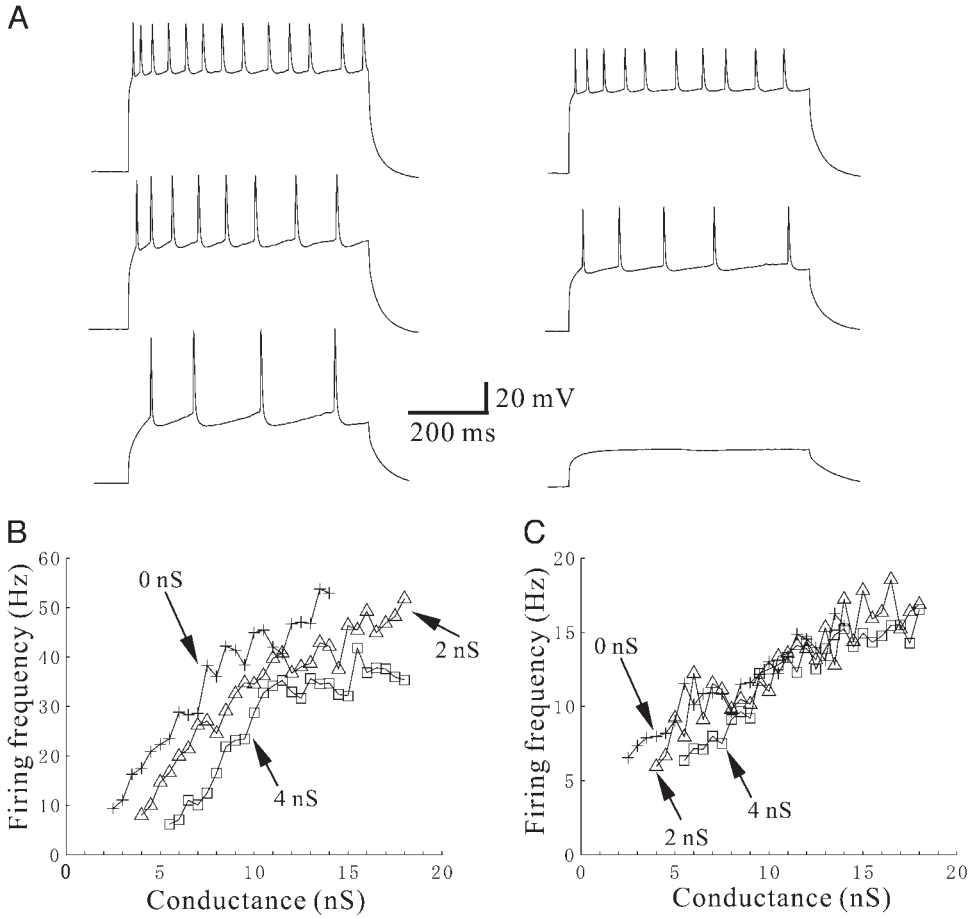

FIG. 5. Frequency-conductance (*f–g*) relationship of an RS neuron. *A*: firing at 3 different levels of AMPA receptor type conductance ($E_{rev} = -10$ mV): 2.5, 6.0, and 9.0 nS. *Left traces*: without shunting inhibition. *Right traces*: with 4-nS shunting inhibitory conductance. High levels of conductance input lead to a high plateau potential with relatively small amplitude spikes. *B*: *f–g* relationship for initial firing rate at 3 different levels of GABA-type inhibitory conductance. Initial firing rate is plotted as a function of the AMPA receptor-type conductance level. Regular firing starts at the lowest value measurable, about 5 Hz. Addition of inhibitory conductance produces a rightward shift of the initial *f–g* relationship. *C*: SS *f–g* relationship. SS firing frequency is plotted against AMPA receptor-type conductance level. Addition of shunting conductance produces a rightward shift of the *f–g* relationship preferentially at lower excitatory conductance levels.

lation, repetitive firing was supported at frequencies as low as could be assessed given the stimulus duration.

FS cell firing also showed the same qualitative pattern with conductance stimulation as with current stimulation, with AMPA-only (Fig. 6*A*, *left*) or AMPA + GABA stimulation (Fig. 6*A*, *right*). Both initial instantaneous (Fig. 6*B*) and SS (Fig. 6*C*) *f–g* relationships showed high nonlinearity, and unlike RS neurons, both were strongly shifted by shunting inhibition. As with current stimulation, a clear type 2 minimum firing frequency or critical frequency (f_c), in the range 20–30 Hz, was observed. It was notable that increasing shunting inhibition increased f_c, for example, from 20 to 30 Hz in the case of the cell in Fig. 6*C*.

Subthreshold oscillations in FS neurons

Particularly with conductance stimulation, it was common in FS cells, but never in RS cells, to find intermittent switching between periodic firing at 20–30 Hz and silence on the edge of threshold (Fig. 6*A*, *right*, *middle trace*). This was also observed over a narrow range with current stimulation. Such irregular firing was excluded from *f–g* or *f–I* relationships, which are restricted to firing that is periodic throughout the test pulse period. This type of firing is a further indication of a type 2 discontinuity in the frequency–stimulus relationship at threshold.

The interruptions in periodic spiking during this unstable irregular bursting of FS neurons were clearly associated with small subthreshold oscillations (Fig. 7*A*). These oscillations showed a strong peak in power spectral density, which matched the threshold spike frequency. An example is shown in Fig. 7*B*, where the subthreshold frequency was about 20 Hz. In 13 different cells, the relationship between spiking and subthreshold oscillation was usually 1:1, although 2:1 oscillations were occasionally observed (Fig. 7*C*).

Stochastic input in the excitable regime

It is widely appreciated that the massive synaptic bombardment received by neurons in vivo represents a strong source of noise. We investigated whether such noisy input has a different effect on the 2 types of cells at firing threshold. For the sake of simplicity, we used a simple white-noise stochastic current input to examine the threshold behaviors of 2 types of neurons rather than a synaptic waveform-based stochastic input (Chance et al. 2002; Harsch and Robinson 2000; Mitchell and Silver 2003).

Figure 8*A* shows the responses of a type 1 cell driven by 3 intensity levels of the noisy current input ($\sigma = 10$, 50, and 100 pA) with a constant (subthreshold) current ($I = 85$ pA) in the excitable regime, such that the cell is silent in the absence of the noise term. As the noise intensity increases, the average firing frequency monotonically increases from a very low firing frequency in all 5 cells, as shown in Fig. 8*B*. This result resembled the *f–I* curves shown in Fig. 4*B*. We quantified the degree of response variability of the type 1 neurons by measuring the coefficient of variation (CV) of the interspike intervals. Figure 8*C* shows average CV versus noise intensity plots

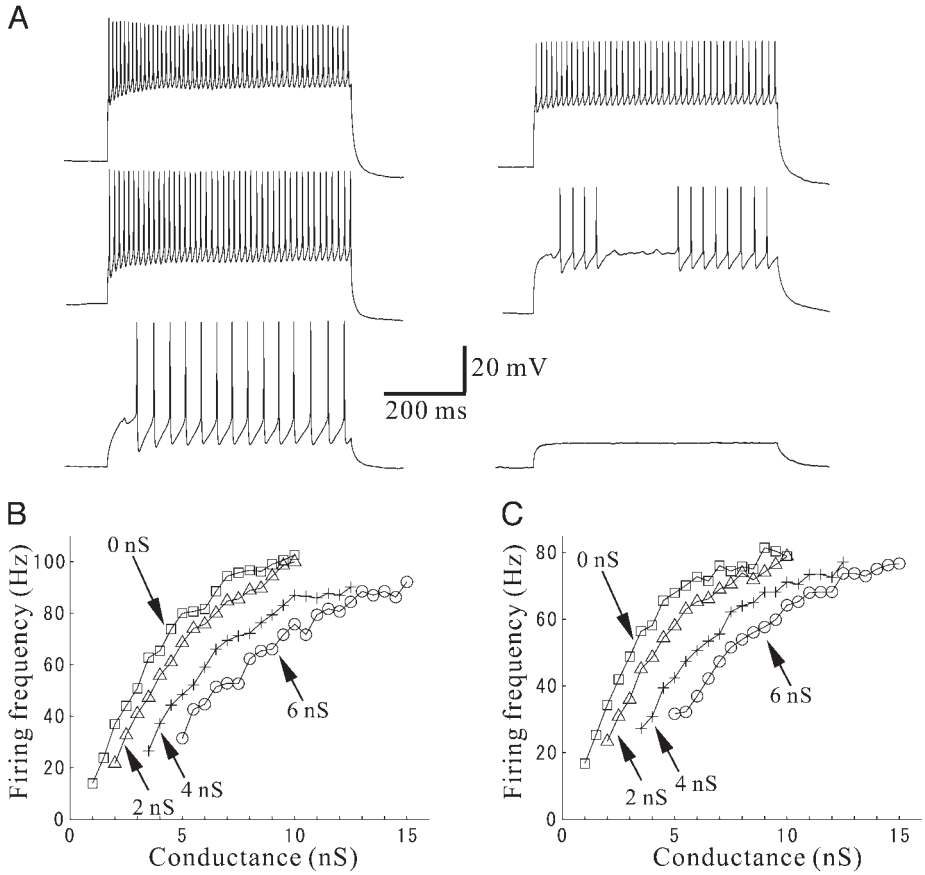

FIG. 6. Frequency-conductance (*f–g*) relationship of an FS neuron. *A*: firing at different levels of AMPA receptor type conductance ($E_{rev} = -10$ mV): 1.5, 5.0, and 10.0 nS. *Left*: without shunting inhibitory conductance. *Right*: with 6-nS shunting inhibitory conductance. Note the abrupt onset of relatively high frequency firing, causing intermittent bursts near the threshold (*middle trace, right*). High levels of conductance lead to a high plateau potential with relatively small amplitude spikes. *B*: *f–g* relationship for initial firing rate at 3 different levels of GABA-type inhibitory conductance. Initial firing rate is plotted as a function of the AMPA receptor-type conductance level. As in the *f–I* relationship (Fig. 4*D*), periodic firing starts at around 20 Hz. Addition of inhibitory conductance produces a rightward shift of the initial *f–g* relationship. *C*: SS *f–g* relationships. Firing frequency is plotted against AMPA receptor-type conductance level. Addition of shunting conductance produces a rightward shift of both initial and SS *f–g* relationships and an increase in f_c.

for 5 different cells in their excitable regimes. In each case, CV first *decreases* with increasing σ, reaching a minimum at an optimum value, and then increases. Because smaller values of CV mean coherence of oscillations (note that in the case of periodic oscillations, CV = 0), such a minimum represents a "coherence resonance" (Pikovsky and Kurths 1997).

Figure 9*A* shows 3 responses of a type 2 FS cell driven by 3 levels of noise intensity (σ = 10, 50, and 120 pA) with a constant current (I = 70 pA). At the lowest noise level in Fig. 9*A*, subthreshold oscillations predominate over suprathreshold spike activity (*top panel*). Although monotonically increasing, *f–σ* relationships for 5 cells were discontinuous at low frequencies and flatter than those of RS cells (Fig. 9*B*). Such properties are also reminiscent of the *f–I* curves shown in Fig. 4*D*, but blurred by the stochastic input. Figure 9*C* shows average CV versus noise intensity plots for 5 different cells in their excitable regimes. In each case, there is a decrease in CV toward a minimum with increasing σ, followed by a slight increase at high σ. Thus coherence resonance also occurs in the type 2 case, but oscillations were more coherent over a wider range of noise intensities.

DISCUSSION

Herein we have examined in detail the threshold region of the relationship between stimulus level and firing frequency, and shown that 2 major functional types of neurons in the cortex, regular-spiking neurons and fast-spiking neurons, have different types of threshold behavior. In previous studies of *f–I* relationships in cortex (Erisir et al. 1999; Nowak et al. 2003), the emphasis has been on mapping the entire relationship, and the current increments used around threshold have not exposed the qualitative distinction between RS and FS neurons. However, Kawaguchi and Erisir et al. reported an "abrupt onset" of firing in FS neurons (Erisir et al. 1999; Kawaguchi 1995). In the present study, the granularity of the stimulus current steps was set as fine as possible, consistent with obtaining repeatable results from trial to trial. A further constraint was the recording time required for very fine increments in stimulus. We also showed that the same type of relationship between stimulus and firing frequency holds for conductance input, where the natural effects of shunting and reduced time constant associated with synaptic input are reproduced, over a range of levels of background inhibition. Background inhibitory conductance caused a rightward shift in the *f–g* relationship, as would be expected for static conductance input (Mitchell and Silver 2003). In addition, we have shown that the same type of relationship holds for white Gaussian noise current input, where the basic features of the noise-free *f–I* relationship are retained, but blurred, in the *f–σ* relationship.

A number of theoretical studies have characterized bifurcations of neural models from the standpoint of the geometrical theory of (nonlinear) dynamical systems (Izhikevich 2000 and references therein). Bifurcation describes a qualitative change in dynamics that can be observed as a system parameter varies (Guckenheimer and Holmes 1983). The difference between type 1 and type 2 is well understood in dynamical models of spike generation (Fig. 10). For example, the Connor et al. model of molluscan neurons shows a type 1 *f–I* relationship (Fig. 10*A*), a consequence of the A-type K^+ current that

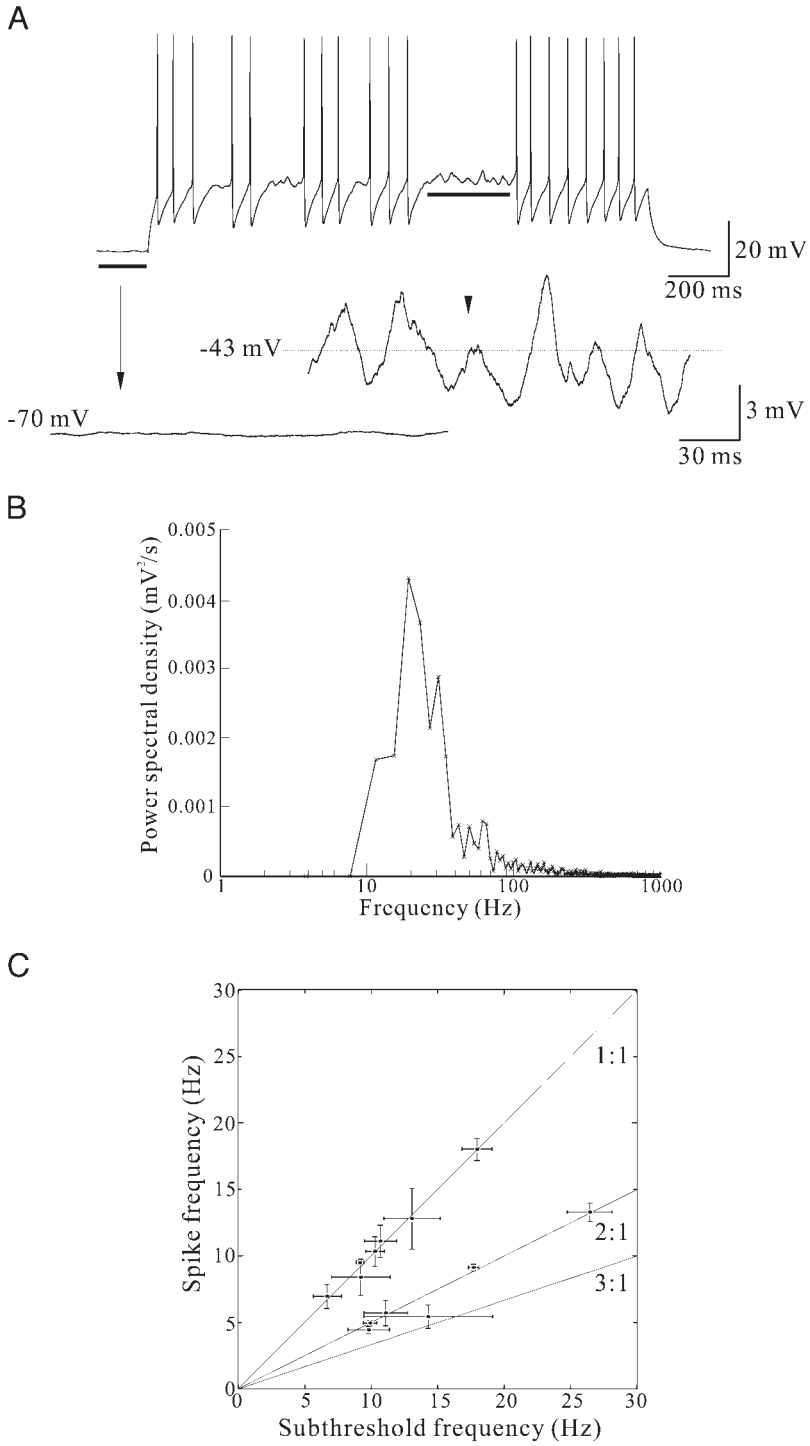

FIG. 7. Subthreshold oscillations in FS neurons. *A*: intermittent alternation between regular firing and subthreshold oscillation near the threshold (60-pA current stimulation). *Inset*: expanded view of subthreshold oscillations as indicated. *B*: power spectral density of subthreshold oscillations peaks at 20 Hz, equal to the threshold spike frequency. *C*: 1:1 relationship between threshold spike and subthreshold oscillation frequencies at the threshold. Data pooled from 13 cells; each symbol represents one cell.

activates rapidly near to rest (Connor et al. 1977), whereas the Hodgkin–Huxley model of squid giant axon (Hodgkin and Huxley 1952) has type 2 behavior (Fig. 10*B*). These models have 6 and 4 dynamical variables, respectively, but the essence of type 1 and type 2 behavior may be understood with 2 variables, as in the FitzHugh–Nagumo (FitzHugh 1961; Nagumo et al. 1962) or Morris–Lecar (Morris and Lecar 1981) models, in which one variable represents voltage and Na^+ or Ca^{2+} channel activation, and one represents Na^+ channel inactivation/K^+ channel activation. At a particular stimulus level, each of these variables has a voltage-dependent derivative, defining a 2-D vector field in the phase plane.

Threshold corresponds to a bifurcation of the dynamics, where a stationary state disappears or becomes unstable, and a stable limit cycle, a closed-loop trajectory, appears as the stimulus is increased. Type 1 models such as the Morris–Lecar type 1 model (Fig. 10*C*) show a saddle-node bifurcation, where the zero-derivative stationary points coalesce and disappear to create a limit cycle. As it passes through the "ghost" of the disappeared stationary points, the limit cycle can experience

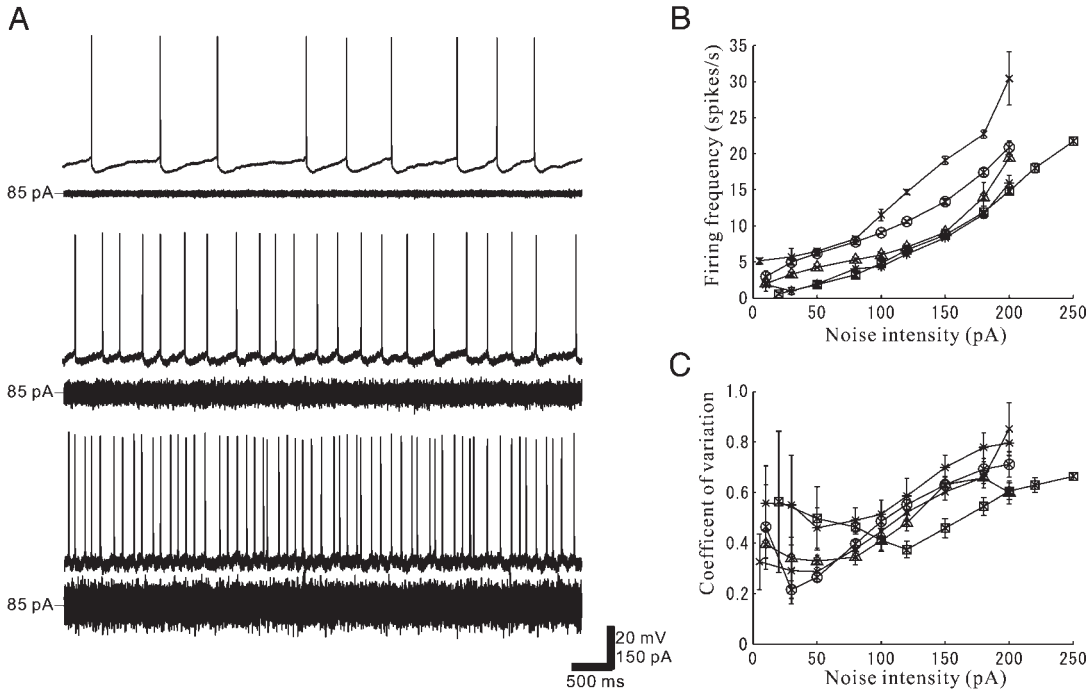

FIG. 8. Responses of RS neurons driven by a stochastic (white-noise) input. *A*: typical responses of an RS cell for 3 different noise intensities (*top*, 10 pA; *middle*, 50 pA; *bottom*, 100 pA) and a subthreshold current (85 pA). *B*: average frequency vs. noise intensity (*f–s*) curves for 5 different RS neurons. Error bars show SDs for 20–30 trials with different noise realizations. *C*: average coefficient of variation (CV) of interspike intervals vs. noise intensity relationship of 5 different RS neurons. Error bars show SDs of CVs for 20–30 trials with different noise realizations.

arbitrarily slow derivatives, and therefore supports periodic firing of arbitrarily low frequency—a continuous *f–I* curve. In contrast, type 2 neural models, such as the Morris–Lecar type 2 (Fig. 10*D*) or FitzHugh–Nagumo models, undergo a subcritical Hopf bifurcation, in which as the stimulus level increases, a stable stationary point becomes unstable, and the trajectory spirals out to find a *preexisting* limit cycle—thus jumping abruptly to a finite firing frequency. Type 2 models such as this

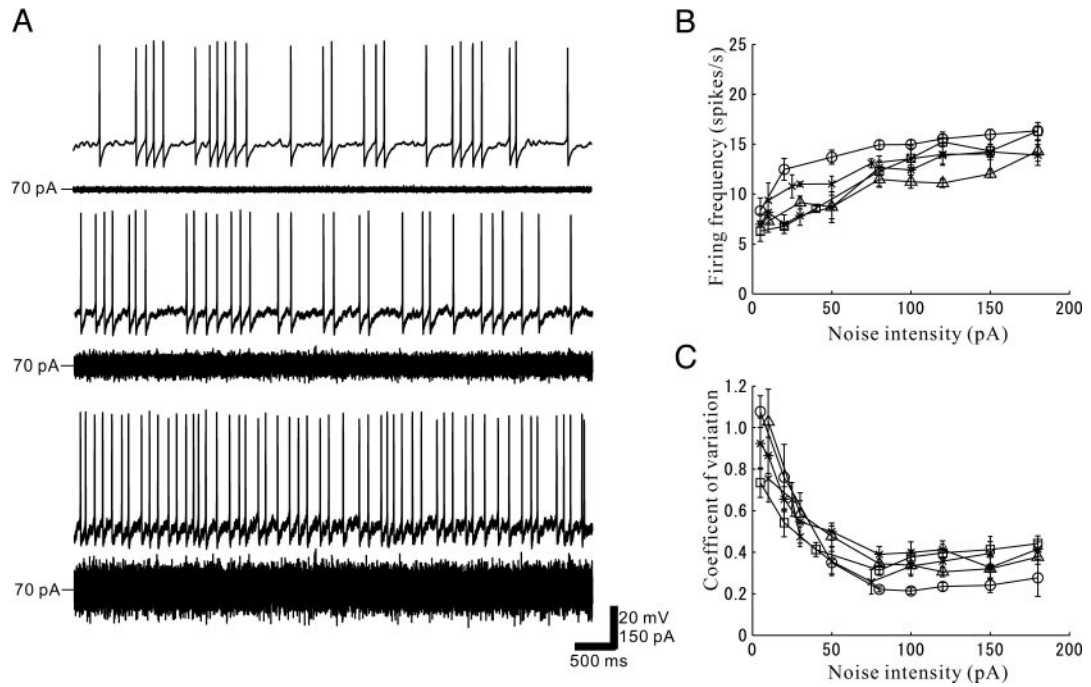

FIG. 9. Responses of FS neurons driven by a stochastic input. *A*: typical responses of an FS cell for 3 different noise intensity (*top*, 10 pA; *middle*, 50 pA; *bottom*, 120 pA) with a subthreshold current (70 pA). *B*: average *f–σ* curves for 5 different FS neurons. Error bars show SDs for 20–30 trials of different noise realization. *C*: average coefficient of variation (CV) of interspike intervals vs. noise intensity relationship of 5 different FS neurons. Error bars show SDs of CVs for 20–30 trials for different noise realizations.

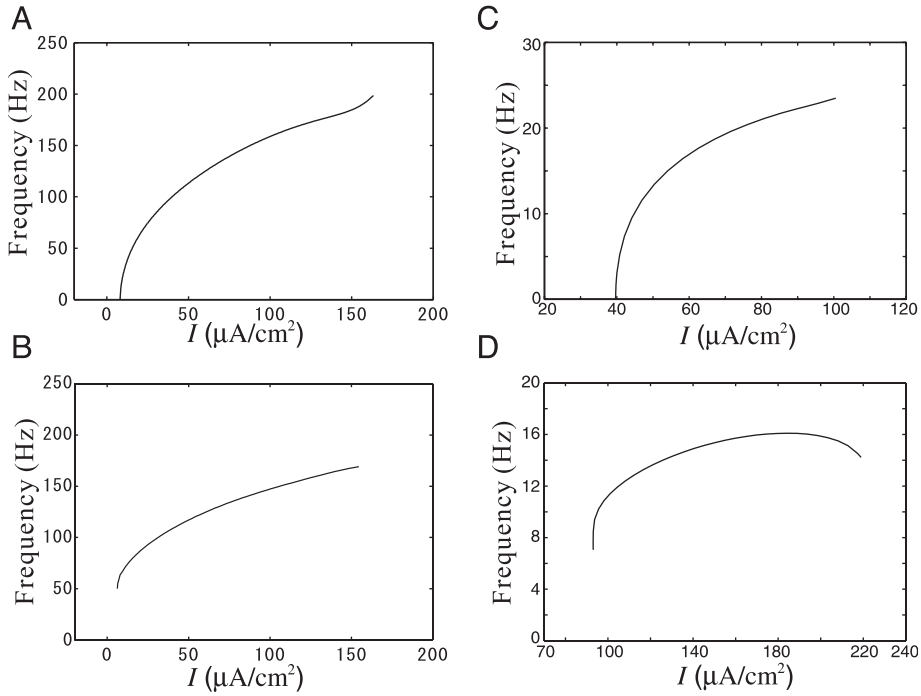

FIG. 10. *f–I* curves for simple models of type 1 and type 2 behavior. *A*: 6-variable Connor et al. model of molluscan neuron, incorporating A-type K^+ conductance, showing type 1 behavior (Connor et al. 1977). *B*: 4-variable Hodgkin–Huxley model of the squid giant axon membrane patch, showing type 2 behavior (Hodgkin and Huxley 1952). *C*: 2-variable Morris–Lecar model with type 1 parameters (Morris and Lecar 1981). *D*: Morris–Lecar model with type 2 parameters.

show subthreshold oscillations at essentially the same frequency as suprathreshold spiking, as we have also observed in FS neurons (Fig. 7) but not in RS neurons. Similar subthreshold oscillations were previously described in interneurons by Llinas et al. (1991) and by Fellous et al. (2001).

Thus this is a further reason for our classification of FS neurons as type 2. Although the bifurcations described above are the most typical ones encountered in lower-dimensional neural models, the mechanism of transition from rest to oscillatory activity in neurons is not restricted to these. Our aim here is not to identify the precise type but to illustrate the feasibility of such bifurcations in lower-dimensional models. Because higher-dimensional spiking models may often be accurately reduced into fast and slow systems of variables, such type 1 and 2 threshold bifurcations may apply quite generally to biological neurons. The noise sensitivity and variability of interspike intervals also strongly depend on the dynamical type. Figure 11 shows CVs of interspike intervals of the ML model driven by white Gaussian noise input on the I_0–σ plane, for type 1 (Fig. 11*A*) and type 2 (Fig. 11*B*) parameters. In the excitable regime ($I < 40$ μA/cm^2) the type 1 ML model shows relatively large CVs (>0.4), whereas it exhibits coherent oscillations (CV < 0.2) only in the oscillatory regime ($I > 40$ μA/cm^2) with small noise ($0 < \sigma < 2$ μA/cm^2). In contrast, the type 2 ML model shows smaller CVs over a larger region of the I_0–σ plane (Fig. 11*B*), demonstrating that coherent oscillations are easily achieved over a wide range of noise intensities even in the excitable regime ($I < 88$ μA/cm^2).

Why is the nature of the threshold region functionally

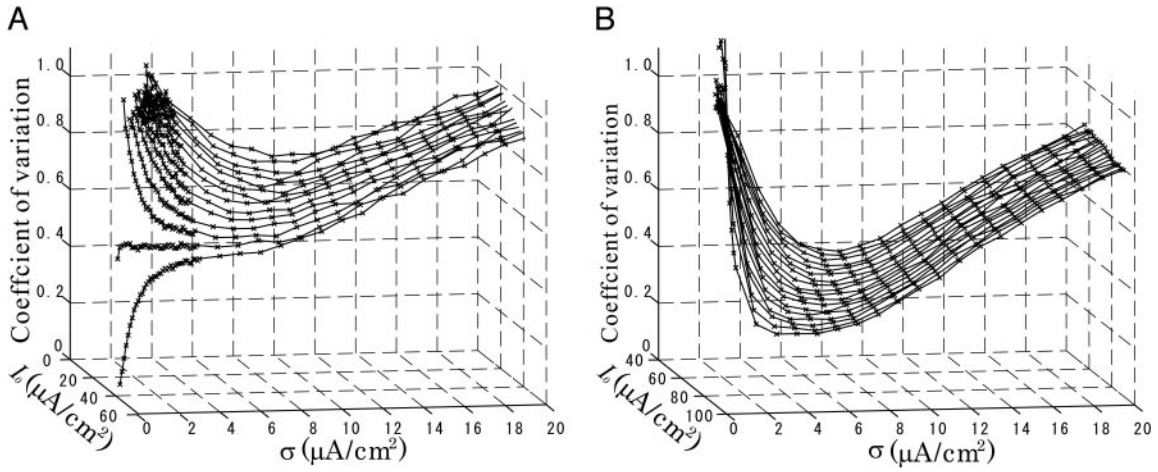

FIG. 11. Average CVs on the I_0–σ plane for the Morris–Lecar model driven by white Gaussian noise. *A*: type 1 parameters. The deterministic (noiseless) system has a stable fixed point and is excitable for $I < 40$ (μA/cm^2). Beyond the bifurcation point ($I = 40$ μA/cm^2) the noiseless system is oscillatory as shown in Fig. 10*C*. *B*: type 2 parameters. For the noiseless system, the double limit bifurcation and subcritical Hopf bifurcation points are at $I = 88.28$ and $I = 93.86$ (μA/cm^2), respectively. See Rinzel and Ermentrout (1998) and Tateno and Pakdaman (2004) for further explanation.

important, when it corresponds to only a small range of stimulus levels? There are several reasons. First, threshold behavior establishes the beginning of responses and therefore must be critical in determining the trajectory of network activity. Second, the fast self-limitation of network activity through mechanisms such as spike adaptation and synaptic depression effectively means that the stimulus level is "balanced" to fluctuate around threshold. Third, many studies show that noise acts most powerfully by far at the threshold (e.g., Lecar and Nossal 1971; Schneidman et al. 1998)—the variability of neuronal firing will be dominated by the behavior at threshold. Type 1 and 2 models have very different noise sensitivities (Gutkin and Ermentrout 1998; Robinson and Harsch 2002). Fluctuation of the stimulus level below threshold type 1 neurons—as their dynamics slow down critically at the threshold—easily and rapidly allows spike generation to become effectively noise-dominated (Poisson).

What is the likely relevance of this to the operation of the cortex? Pyramidal RS cells appear to associate inputs from different layers and areas in the cortex, by the back-propagation–activated dendritic calcium-spike mechanism (Larkum et al. 1999). Type 1 behavior of RS neurons might allow relatively easy switching between different tempos in their inputs. It may also promote the generally high level of firing variability in the cortex, as suggested by Gutkin and Ermentrout (1998)—probably over 50% of cortical cells are type 1 RS neurons. RS neurons are, by virtue of their type 1 dynamics, suited to encoding even low stimulus levels in the firing rate (i.e., as randomized, Poisson-process–like firing); this may have advantages for network stability, by breaking up exact synchrony.

On the other hand, type 2 FS neurons, which inhibit each other and other RS neurons locally (Holmgren et al. 2003), are implicated in promoting episodes of synchronous firing (Beierlein et al. 2000; Galarreta and Hestrin 2001). They are coupled together by electrical synapses or gap junctions, which helps to synchronize their action potentials precisely (Gibson et al. 1999). The nature of type 2 dynamics may mean that the phase of rhythmic firing is quite stable even when the mean stimulus goes subthreshold because strong subthreshold oscillations could keep the rhythm intact until the stimulus moves above threshold again: there is fast motion below threshold. For a type 2 neuron, there is a much greater tendency for spikes to drop out without a consequent wide dispersion of spike times as the stimulus passes below threshold (Robinson 2004). In other words, type 2 neurons intrinsically prefer to stay coherent with their input or to be silent, whereas type 1 neurons have a graded transition between the 2 extremes. The identity of subthreshold oscillation and suprathreshold spike frequency (f_c) for FS neurons could lead to stable synchronous oscillations at 20–30 Hz, as have been suggested to be important in sensory feature recognition and binding (Singer and Gray 1995). The increase in f_c produced by GABAergic input, as shown in Fig. 6*C*, could provide a mechanism for a physiological modulation of this synchronous firing frequency.

Computational modeling provides some support for the scenarios described above; the dynamics of coupled neurons and of neural networks critically depend on their excitability types. For example, Hansel et al. (1995) showed that excitatory synapses cannot lead to synchronization for type 1 neural models like the Connor et al. model unless the synapses are very fast. Hansel et al. also showed numerically that type 2 excitability can easily lead to synchronization of coupled oscillations, using the Hodgkin–Huxley model. In addition, Ermentrout (1996) reported that, compared with type 2 models, synchrony is in general difficult to achieve when oscillators have type 1 excitability.

In conclusion, there are two types of threshold behavior for periodically firing neurons, which show continuous (type 1) or discontinuous (type 2) *f–I* curves. We have shown that in the cortex, regular-spiking and fast-spiking neuronal types have type 1 and type 2 thresholds, respectively. This endows them with fundamentally different spike rate encoding, noise sensitivity, subthreshold, and synchronization properties. Thus they are expected to serve very different roles in the dynamics of the cortical network.

ACKNOWLEDGMENTS

One of the authors (T. Tateno) thanks Professor Shunsuke Sato and Professor Taishin Nomura (Osaka University) for their support and encouragement.

GRANTS

This work was supported in part by the Japanese Society for the Promotion of Science (JSPS) Postdoctoral Fellowships for Research Abroad, the Biotechnology and Biological Sciences Research Council, and the European Coumcil.

REFERENCES

Arvanitaki A. Recherches sur la reponse oscillatoire locale de laxone geant isole de "sepia." *Arch Int Physiol* 49: 209–256, 1936.

Beierlein M, Gibson JR, and Connors BW. A network of electrically coupled interneurons drives synchronized inhibition in neocortex. *Nat Neurosci* 3: 904–910, 2000.

Brink F, Bronk DW, and Larrabee MG. Chemical excitation of nerve. *Ann NY Acad Sci* 47: 457–485, 1946.

Connor JA, Walter D, and McKown R. Modifications of the Hodgkin–Huxley axon suggested by experimental results from crustacean axons. *Biophys J* 18: 81–102, 1977.

Connors BW and Gutnick MJ. Intrinsic firing patterns of diverse neocortical neurons. *Trends Neurosci* 13: 99–104, 1990.

Connors BW, Gutnick MJ, and Prince DA. Electrophysiological properties of neocortical neurons in vitro. *J Neurophysiol* 48: 1302–1320, 1982.

Destexhe A, Rudolph M, Fellous J-M, and Sejnowski TJ. Fluctuating synaptic conductances recreate in-vivo-like activity in neocortical neurons. *Neuroscience* 107: 13–24, 2001.

Doedel E and Kernevez JP. *AUTO: Software for Continuation and Bifurcation Problems in Ordinary Differential Equations*, Applied Mathematics Report. Pasadena, CA: California Institute of Technology, 1986.

Erisir A, Lau D, Rudy B, and Leonard CS. Function of specific K channels in sustained high-frequency firing of fast-spiking neocortical interneurons. *J Neurophysiol* 82: 2476–2489, 1999.

Ermentrout B. Type 1 membrane, phase resetting curves, and synchrony. *Neural Comput* 8: 979–1002, 1996.

Ermentrout B. Linearization of F–I curves by adaptation. *Neural Comput* 10: 1721–1729, 1998.

Ermentrout B. *Simulating, Analyzing, and Animating Dynamical Systems: A Guide to XPPAUT for Researchers and Students.* Philadelphia, PA: Society for Industrial and Applied Mathematics (SIAM), 2002.

Fellous JM, Houweling AR, Modi RH, Rao RPN, Tiesinga PHE, and Sejnowski TJ. Frequency dependence of spike timing reliability in cortical pyramidal cells and interneurons. *J Neurophysiol* 85: 1782–1787, 2001.

FitzHugh R. Impulses and physiological states in theoretical models of nerve membrane. *Biophys J* 1: 445–466, 1961.

Galarreta M and Hestrin S. Spike transmission and synchrony detection in networks of GABAergic interneurons. *Science* 292: 2295–2299, 2001.

Gibson JR, Beierlin M, and Connors BW. Two networks of electrically coupled inhibitory neurons in neocortex. *Nature* 402: 75–79, 1999.

Guckenheimer J and Holmes P. *Nonlinear Oscillations, Dynamical Systems, and Bifurcations of Vector Fields.* Berlin: Springer-Verlag, 1983.

Gutfreund Y, Yarom Y, and Segev I. Subthreshold oscillations and resonant frequency in guinea-pig cortical neurons: physiology and modelling. *J Physiol* 483: 621–640, 1995.

Gutkin B and Ermentrout B. Dynamics of membrane excitability determine interspike interval variability: a link between spike generation and cortical spike train statistics. *Neural Comput* 10: 1047–1065, 1998.

Hansel D, Mato G, and Meunier C. Synchrony in excitatory neural networks. *Neural Comput* 7: 307–337, 1995.

Hodgkin AL. The local electric changes associated with repetitive action in a non-medullated axon. *J Physiol* 107: 165–181, 1948.

Hodgkin AL and Huxley AF. A quantitative description of membrane current and its application to conduction and excitation in nerve. *J Physiol* 463: 391–407, 1952.

Holmgren C, Harkany T, Svennenfors B, and Zilberter Y. Pyramidal cell communication within local networks in layer 2/3 of rat neocortex. *J Physiol* 551: 139–153, 2003.

Izhikevich EM. Neural excitability, spiking and bursting. *Int J Bifurcation Chaos* 10: 1171–1266, 2000.

Kawaguchi Y. Physiological subgroups of nonpyramidal cells with specific morphological characteristics in layer II/III of rat frontal cortex. *J Neurosci* 15: 2638–2655, 1995.

Kawaguchi Y and Kubota Y. GABAergic cell subtypes and their synaptic connections in rat frontal cortex. *Cereb Cortex* 7: 476–486, 1997.

Kloeden PE and Platen E. *Numerical Solution of Stochastic Differential Equations*. Berlin: Springer-Verlag, 1999.

Larkum ME, Kaiser KMM, and Sakmann B. Calcium electrogenesis in distal apical dendrites of layer 5 pyramidal cells at a critical frequency of back-propagating action potentials. *Proc Natl Acad Sci USA* 96: 14600–14604, 1999.

Lecar H and Nossal R. Theory of threshold fluctuations in nerves. I. Relationships between electrical noise and fluctuations in axon firing. *Biophys J* 11: 1048–1067, 1971.

Llinas RR, Grace AA, and Yarom Y. In vitro neurons in mammalian cortical layer 4 exhibit intrinsic oscillatory Activity in the 10- to 50-Hz frequency range. *Proc Natl Acad Sci USA* 88: 897–901, 1991.

Mitchell SJ and Silver RA. Shunting inhibition modulates neuronal gain during synaptic excitation. *Neuron* 38: 433–445, 2003.

Morris C and Lecar H. Voltage oscillations in the barnacle giant muscle fibre. *Biophys J* 35: 193–213, 1981.

Nagumo JS, Arimoto S, and Yoshizawa S. An active pulse transmission line stimulating a nerve axon. *Proceedings IRE* 50: 2061–2070, 1962.

Nowak LG, Azouz R, Sanchez-Vives MV, Gray CM, and McCormick DA. Electrophysiological classes of cat primary visual cortical neurons in vivo as revealed by quantitative analyses. *J Neurophysiol* 89: 1541–1566, 2003.

Pike FG, Goddard RS, Suckling JM, Ganter P, Kasthuri N, and Paulsen O. Distinct frequency preferences of different types of rat hippocampal neurones in response to oscillatory input currents. *J Physiol* 529: 205–213, 2000.

Pikovsky AS and Kurths J. Coherence resonance in a noise-driven excitable system. *Phys Rev Lett* 78: 775–778, 1997.

Rinzel J and Ermentrout B. Analysis of neural excitability and oscillations. In: *Methods in Neuronal Modelling*: *From Ions to Networks*, edited by Koch C and Segev I. Cambridge, MA: MIT Press, 1998, p. 251–291.

Robinson HPC. The biophysical basis of firing variability in cortical neurons. In: *Computational Neuroscience*: *A Comprehensive Approach*, edited by Feng JF. London: CRC LLC, 2004, p. 159–183.

Robinson HPC and Harsch A. Stages of spike time variability during neuronal responses to transient inputs. *Phys Rev E* 66: 061902, 2002.

Robinson HPC and Kawai N. Injection of digitally synthesized synaptic conductance transients to measure the integrative properties of neurons. *J Neurosci Methods* 49: 157–165, 1993.

Sakmann B and Stuart G. Patch-pipette recordings from the soma, dendrites and axon of neurons in brain slices. In: *Single-Channel Recording*, edited by Sakmann B and Neher E. New York: Plenum, 1995, p. 199–211.

Schneidman E, Freedman B, and Segev I. Ion channel stochasticity may be critical in determining the reliability and precision of spike timing. *Neural Comput* 10: 1679–1703, 1998.

Sharp AA, O'Neil MB, Abbott LF, and Marder E. Dynamic clamp: computer-generated conductances in real neurons. *J Neurophysiol* 69: 992–995, 1993.

Singer W and Gray CM. Visual feature integration and the temporal correlation hypothesis. *Ann Rev Neurosci* 18: 555–586, 1995.

Tateno T and Pakdaman K. Random dynamics of the Morris–Lecar neural model. *Chaos: An Interdisciplinary Journal of Nonlinear Science* 14: 511–530, 2004.